Production of K^0 and Λ in hadronic Z decays

D. Buskulic, D. Casper, I. de Bonis, D. Decamp, P. Ghez, C. Goy, J P. Lees, M N. Minard, P. Odier, B. Pietrzyk, et al.

EUROPEAN ORGANIZATION FOR NUCLEAR RESEARCH

CERN-PPE/94-74
27 May 1994

Production of K^0 and Λ in hadronic Z decays

The ALEPH Collaboration

Abstract

Measurements of the inclusive cross-sections for K^0 and Λ production in hadronic decays of the Z are presented together with measurements of two–particle correlations within pairs of Λ and K^0. The results are compared with predictions from the hadronization models JETSET, based on string fragmentation, and HERWIG, based on cluster decays. The K^0 spectrum is found to be harder than predicted by both models, while the Λ spectrum is softer than predicted. The correlation measurements are all reproduced well by JETSET, while HERWIG misses some of the qualitative features and overestimates the size of the $\Lambda\bar{\Lambda}$ correlation. Finally, the possibility of Bose-Einstein correlation in the $K^0_S K^0_S$ system is discussed.

submitted to *Z.Phys.C*

The ALEPH Collaboration

D. Buskulic, D. Casper, I. De Bonis, D. Decamp, P. Ghez, C. Goy, J.-P. Lees, M.-N. Minard, P. Odier, B. Pietrzyk

Laboratoire de Physique des Particules (LAPP), IN^{2}P^3-CNRS, 74019 Annecy-le-Vieux Cedex, France

F. Ariztizabal, M. Chmeissani, J.M. Crespo, I. Efthymiopoulos, E. Fernandez, M. Fernandez-Bosman, V. Gaitan, Ll. Garrido,[28] M. Martinez, T. Mattison,[29] S. Orteu, A. Pacheco, C. Padilla, A. Pascual, F. Teubert

Institut de Fisica d'Altes Energies, Universitat Autonoma de Barcelona, 08193 Bellaterra (Barcelona), Spain[7]

D. Creanza, M. de Palma, A. Farilla, G. Iaselli, G. Maggi, N. Marinelli, S. Natali, S. Nuzzo, A. Ranieri, G. Raso, F. Romano, F. Ruggieri, G. Selvaggi, L. Silvestris, P. Tempesta, G. Zito

Dipartimento di Fisica, INFN Sezione di Bari, 70126 Bari, Italy

Y. Chai, D. Huang, X. Huang, J. Lin, T. Wang, Y. Xie, D. Xu, R. Xu, J. Zhang, L. Zhang, W. Zhao

Institute of High-Energy Physics, Academia Sinica, Beijing, The People's Republic of China[8]

G. Bonvicini, J. Boudreau,[25] P. Comas, P. Coyle, H. Drevermann, A. Engelhardt, R.W. Forty, G. Ganis, C. Gay,[3] M. Girone, R. Hagelberg, J. Harvey, R. Jacobsen, B. Jost, J. Knobloch, I. Lehraus, M. Maggi, C. Markou, P. Mato, H. Meinhard, A. Minten, R. Miquel, P. Palazzi, J.R. Pater, J.A. Perlas, P. Perrodo, J.-F. Pusztaszeri, F. Ranjard, L. Rolandi, J. Rothberg,[2] M. Saich, D. Schlatter, M. Schmelling, F. Sefkow,[6] W. Tejessy, I.R. Tomalin, R. Veenhof, A. Venturi, H. Wachsmuth, S. Wasserbaech,[2] W. Wiedenmann, T. Wildish, W. Witzeling, J. Wotschack

European Laboratory for Particle Physics (CERN), 1211 Geneva 23, Switzerland

Z. Ajaltouni, M. Bardadin-Otwinowska, A. Barres, C. Boyer, A. Falvard, P. Gay, C. Guicheney, P. Henrard, J. Jousset, B. Michel, J-C. Montret, D. Pallin, P. Perret, F. Podlyski, J. Proriol, F. Saadi

Laboratoire de Physique Corpusculaire, Université Blaise Pascal, IN^{2}P^3-CNRS, Clermont-Ferrand, 63177 Aubière, France

T. Fearnley, J.B. Hansen, J.D. Hansen, J.R. Hansen, P.H. Hansen, S.D. Johnson, R. Møllerud, B.S. Nilsson

Niels Bohr Institute, 2100 Copenhagen, Denmark[9]

A. Kyriakis, E. Simopoulou, I. Siotis, A. Vayaki, K. Zachariadou

Nuclear Research Center Demokritos (NRCD), Athens, Greece

J. Badier, A. Blondel, G. Bonneaud, J.C. Brient, P. Bourdon, G. Fouque, L. Passalacqua, A. Rougé, M. Rumpf, R. Tanaka, A. Valassi, M. Verderi, H. Videau

Laboratoire de Physique Nucléaire et des Hautes Energies, Ecole Polytechnique, IN^{2}P^3-CNRS, 91128 Palaiseau Cedex, France

D.J. Candlin, M.I. Parsons, E. Veitch

Department of Physics, University of Edinburgh, Edinburgh EH9 3JZ, United Kingdom[10]

E. Focardi, G. Parrini

Dipartimento di Fisica, Università di Firenze, INFN Sezione di Firenze, 50125 Firenze, Italy

M. Corden, M. Delfino,[12] C. Georgiopoulos, D.E. Jaffe, D. Levinthal[15]

Supercomputer Computations Research Institute, Florida State University, Tallahassee, FL 32306-4052, USA [13,14]

A. Antonelli, G. Bencivenni, G. Bologna,[4] F. Bossi, P. Campana, G. Capon, F. Cerutti, V. Chiarella, G. Felici, P. Laurelli, G. Mannocchi,[5] F. Murtas, G.P. Murtas, M. Pepe-Altarelli, S. Salomone

Laboratori Nazionali dell'INFN (LNF-INFN), 00044 Frascati, Italy

P. Colrain, I. ten Have, I.G. Knowles, J.G. Lynch, W. Maitland, W.T. Morton, C. Raine, P. Reeves, J.M. Scarr, K. Smith, M.G. Smith, A.S. Thompson, S. Thorn, R.M. Turnbull

Department of Physics and Astronomy, University of Glasgow, Glasgow G12 8QQ,United Kingdom[10]

U. Becker, O. Braun, C. Geweniger, P. Hanke, V. Hepp, E.E. Kluge, A. Putzer,[1] B. Rensch, M. Schmidt, H. Stenzel, K. Tittel, M. Wunsch

Institut für Hochenergiephysik, Universität Heidelberg, 69120 Heidelberg, Fed. Rep. of Germany[16]

R. Beuselinck, D.M. Binnie, W. Cameron, M. Cattaneo, D.J. Colling, P.J. Dornan, J.F. Hassard, N. Konstantinidis, L. Moneta, A. Moutoussi, J. Nash, D.G. Payne, G. San Martin, J.K. Sedgbeer, A.G. Wright

Department of Physics, Imperial College, London SW7 2BZ, United Kingdom[10]

P. Girtler, D. Kuhn, G. Rudolph, R. Vogl

Institut für Experimentalphysik, Universität Innsbruck, 6020 Innsbruck, Austria[18]

C.K. Bowdery, T.J. Brodbeck, A.J. Finch, F. Foster, G. Hughes, D. Jackson, N.R. Keemer, M. Nuttall, A. Patel, T. Sloan, S.W. Snow, E.P. Whelan

Department of Physics, University of Lancaster, Lancaster LA1 4YB, United Kingdom[10]

A. Galla, A.M. Greene, K. Kleinknecht, J. Raab, B. Renk, H.-G. Sander, H. Schmidt, S.M. Walther, R. Wanke, B. Wolf

Institut für Physik, Universität Mainz, 55099 Mainz, Fed. Rep. of Germany[16]

A.M. Bencheikh, C. Benchouk, A. Bonissent, D. Calvet, J. Carr, C. Diaconu, F. Etienne, D. Nicod, P. Payre, L. Roos, D. Rousseau, P. Schwemling, M. Talby

Centre de Physique des Particules, Faculté des Sciences de Luminy, IN^{2}P^3-CNRS, 13288 Marseille, France

S. Adlung, R. Assmann, C. Bauer, W. Blum, D. Brown, P. Cattaneo,[23] B. Dehning, H. Dietl, F. Dydak,[21] M. Frank, A.W. Halley, K. Jakobs, H. Kroha, J. Lauber, G. Lütjens, G. Lutz, W. Männer, H.-G. Moser, R. Richter, S. Schael, J. Schröder, A.S. Schwarz, R. Settles, H. Seywerd, U. Stierlin,[30] U. Stiegler, R. St. Denis, G. Wolf

Max-Planck-Institut für Physik, Werner-Heisenberg-Institut, 80805 München, Fed. Rep. of Germany[16]

R. Alemany, J. Boucrot, O. Callot, A. Cordier, M. Davier, L. Duflot, J.-F. Grivaz, Ph. Heusse, P. Janot, D.W. Kim,[19] F. Le Diberder, J. Lefrançois, A.-M. Lutz, G. Musolino, M.-H. Schune, J.-J. Veillet, I. Videau

Laboratoire de l'Accélérateur Linéaire, Université de Paris-Sud, IN^{2}P^3-CNRS, 91405 Orsay Cedex, France

D. Abbaneo, G. Bagliesi, G. Batignani, U. Bottigli, C. Bozzi, G. Calderini, M. Carpinelli, M.A. Ciocci, V. Ciulli, R. Dell'Orso, I. Ferrante, F. Fidecaro, L. Foà,[1] F. Forti, A. Giassi, M.A. Giorgi, A. Gregorio, F. Ligabue, A. Lusiani, P.S. Marrocchesi, E.B. Martin, A. Messineo, F. Palla, G. Rizzo, G. Sanguinetti, P. Spagnolo, J. Steinberger, R. Tenchini,[1] G. Tonelli,[27] G. Triggiani, C. Vannini, P.G. Verdini, J. Walsh

Dipartimento di Fisica dell'Università, INFN Sezione di Pisa, e Scuola Normale Superiore, 56010 Pisa, Italy

A.P. Betteridge, Y. Gao, M.G. Green, D.L. Johnson, P.V. March, T. Medcalf, Ll.M. Mir, I.S. Quazi, J.A. Strong

Department of Physics, Royal Holloway & Bedford New College, University of London, Surrey TW20 OEX, United Kingdom[10]

V. Bertin, D.R. Botterill, R.W. Clifft, T.R. Edgecock, S. Haywood, M. Edwards, P.R. Norton, J.C. Thompson

Particle Physics Dept., Rutherford Appleton Laboratory, Chilton, Didcot, Oxon OX11 OQX, United Kingdom[10]

B. Bloch-Devaux, P. Colas, H. Duarte, S. Emery, W. Kozanecki, E. Lançon, M.C. Lemaire, E. Locci, B. Marx, P. Perez, J. Rander, J.-F. Renardy, A. Rosowsky, A. Roussarie, J.-P. Schuller, J. Schwindling, D. Si Mohand, B. Vallage

Service de Physique des Particules, DAPNIA, CE-Saclay, 91191 Gif-sur-Yvette Cedex, France[17]

R.P. Johnson, A.M. Litke, G. Taylor, J. Wear

Institute for Particle Physics, University of California at Santa Cruz, Santa Cruz, CA 95064, USA[22]

A. Beddall, C.N. Booth, S. Cartwright, F. Combley, I. Dawson, A. Koksal, C. Rankin, L.F. Thompson

Department of Physics, University of Sheffield, Sheffield S3 7RH, United Kingdom[10]

A. Böhrer, S. Brandt, G. Cowan,[1] E. Feigl, C. Grupen, G. Lutters, J. Minguet-Rodriguez, F. Rivera,[26] P. Saraiva, U. Schäfer, L. Smolik

Fachbereich Physik, Universität Siegen, 57068 Siegen, Fed. Rep. of Germany[16]

L. Bosisio, R. Della Marina, G. Giannini, B. Gobbo, L. Pitis, F. Ragusa[20]

Dipartimento di Fisica, Università di Trieste e INFN Sezione di Trieste, 34127 Trieste, Italy

L. Bellantoni, J.S. Conway,[24] Z. Feng, D.P.S. Ferguson, Y.S. Gao, J. Grahl, J.L. Harton, O.J. Hayes, H. Hu, J.M. Nachtman, Y.B. Pan, Y. Saadi, M. Schmitt, I. Scott, V. Sharma, J.D. Turk, A.M. Walsh, F.V. Weber,[1] Sau Lan Wu, X. Wu, J.M. Yamartino, M. Zheng, G. Zobernig

Department of Physics, University of Wisconsin, Madison, WI 53706, USA[11]

[1] Now at CERN, PPE Division, 1211 Geneva 23, Switzerland.
[2] Permanent address: University of Washington, Seattle, WA 98195, USA.
[3] Now at Harvard University, Cambridge, MA 02138, U.S.A.
[4] Also Istituto di Fisica Generale, Università di Torino, Torino, Italy.
[5] Also Istituto di Cosmo-Geofisica del C.N.R., Torino, Italy.
[6] Now at DESY, Hamburg, Germany.
[7] Supported by CICYT, Spain.
[8] Supported by the National Science Foundation of China.
[9] Supported by the Danish Natural Science Research Council.
[10] Supported by the UK Science and Engineering Research Council.
[11] Supported by the US Department of Energy, contract DE-AC02-76ER00881.
[12] On leave from Universitat Autonoma de Barcelona, Barcelona, Spain.
[13] Supported by the US Department of Energy, contract DE-FG05-92ER40742.
[14] Supported by the US Department of Energy, contract DE-FC05-85ER250000.
[15] Present address: Lion Valley Vineyards, Cornelius, Oregon, U.S.A.
[16] Supported by the Bundesministerium für Forschung und Technologie, Fed. Rep. of Germany.
[17] Supported by the Direction des Sciences de la Matière, C.E.A.
[18] Supported by Fonds zur Förderung der wissenschaftlichen Forschung, Austria.
[19] Permanent address: Kangnung National University, Kangnung, Korea.
[20] Now at Dipartimento di Fisica, Università di Milano, Milano, Italy.
[21] Also at CERN, PPE Division, 1211 Geneva 23, Switzerland.
[22] Supported by the US Department of Energy, grant DE-FG03-92ER40689.
[23] Now at Università di Pavia, Pavia, Italy.
[24] Now at Rutgers University, Piscataway, NJ 08854, USA.
[25] Now at University of Pittsburgh, Pittsburgh, PA 15260, U.S.A.
[26] Partially supported by Colciencias, Colombia.
[27] Also at Istituto di Matematica e Fisica, Università di Sassari, Sassari, Italy.
[28] Permanent address: Dept. d'Estructura i Constituens de la Materia, Universitat de Barcelona, 08208 Barcelona, Spain.
[29] Now at SLAC, Stanford, CA 94309, U.S.A.
[30] Deceased.

1 Introduction

The spectra of identified particles and two–particle correlations measured in hadronic e^+e^- collisions have in the past been difficult to describe within hadronization models [1]. While the global event properties agree impressively well with model simulations, being to a large extent determined by the perturbative parton shower, the spectra of particular hadrons depend more on the phenomenological part of the models, which is less well understood. Improved measurements may hopefully lead to better understanding of the hadronization process.

This report considers K^0 mesons and Λ hyperons which are relatively easy to identify in the ALEPH apparatus. Measurements of the inclusive spectra are presented, based on 988000 hadronic Z decays collected during 1991 and 1992. Such spectra have previously been studied by OPAL [2, 3], by DELPHI [4, 5] and L3 [6]. In addition, measurements of two–particle correlations among pairs of K^0 and Λ are presented in various projections of rapidity and angle with respect to the thrust axis. Finally, the possibility of Bose–Einstein correlation in the $K^0_S K^0_S$ system is discussed. Similar correlation studies have recently been published by OPAL [7, 8] and DELPHI [5], and the topic of baryon–antibaryon correlations was also studied at PEP and PETRA energies [9, 10, 11].

Two hadronization models have become standard at LEP, the JETSET model [12], implementing a string fragmentation scheme, and the HERWIG model [13], implementing a cluster fragmentation scheme. In both models the overall rate of strange particle production is suppressed by a parameter related to the strange quark effective mass. The shape of the spectra provides additional information which may constrain other parameters of the models. For example, measurements of baryon production have been used to determine the strangeness and spin 1 suppression of diquark states in JETSET. In the default version of HERWIG, however, the flavor and spin ratios are controlled by phase–space only (although the parameters needed to regulate such ratios are actually available).

The parameter space in JETSET is increased by the "popcorn mechanism", allowing a meson to be created in between a baryon–antibaryon pair. This costs an extra parameter specifying the probability for popcorn, and two other ones specifying the strangeness suppression in this case. The rapidity distance between the baryons would appear to be a good probe of such a mechanism.

The results presented in this report are compared with JETSET (version 7.3) and HERWIG (version 5.6) and discussed in terms of the parameters mentioned above.

2 The ALEPH detector

The ALEPH detector has been described in detail elsewhere [14]. For this study it is mainly the tracking capability of the detector that is relevant. Charged tracks are measured over the polar angle range $|\cos\Theta| < 0.966$ by an inner cylindrical drift chamber (ITC) and a large cylindrical time projection chamber (TPC). These chambers are immersed in a magnetic field of 1.5 T and together measure the momentum of charged particles with a resolution of $\delta p/p = 0.0008 \cdot p\,(GeV/c)^{-1} \oplus 0.003$ [14, 15].

Central tracks, with $|\cos\Theta| < 0.85$, are in addition measured by a vertex detector (VDET) [16] consisting of two barrels of multistrip silicon detectors, with double–sided readout, positioned between the beam–pipe and the ITC. The solid angle coverage is 85% for the inner layer and 69% for the outer layer. For high momentum tracks the resolution improves with the addition of the VDET coordinates to $\delta p/p = 0.0006 \cdot p\,(GeV/c)^{-1}$, as measured with di–muon events. The VDET point resolution is 12 μm at normal incidence for both $r\phi$ and rz projections.

The TPC provides up to 330 measurements of the specific ionization ($\mathrm{d}E/\mathrm{d}x$) of each charged track.

For charged tracks with momenta above 3 GeV/c and with the maximum number of samples, the truncated mean ionization of pions and protons are separated by three standard deviations.

3 Event selection and V^0 reconstruction

A sample of hadronic Z decays is defined by a requirement of at least five charged tracks in the event with $|\cos\Theta| < 0.95$ and with a distance to the interaction point of less than 2cm in the transverse direction and 10cm in the longitudinal direction. The charged tracks in the event must carry at least 10% of the collision energy. This selection includes 97.5% of all hadronic Z decays, 0.3% background from τ pairs and 0.4% background from two–photon collisions [17].

All oppositely charged pairs of tracks with momentum larger than 150 MeV/c and with more than 5 TPC coordinates are tested for the hypothesis that they originate from a common secondary vertex. The parameters of the fit are the coordinates of the secondary vertex and the track momenta at this point. Since each track is described by five helix parameters, the fit has one degree of freedom. The chisquared of the fit is required to be less than 13. Such V^0 candidates are then considered that have momentum larger than 200 MeV/c (500 MeV/c for Λ candidates) and polar angle larger than 20°.

In order to ensure a separation between the primary and secondary vertices, the proper lifetime of a given V^0 hypothesis is required to be between 0.2 and 5 times the expected lifetime. Pairs of tracks both originating from the primary vertex are suppressed by requiring that they be separated by at least 0.4cm at their closest approach to the beam–axis in the plane perpendicular to the axis. In addition candidates are rejected for which both tracks have VDET hits between the primary and secondary vertices.

Since the combinatorial background peaks strongly at forward decay angles, the cosine of the decay angle is required to be less than 0.85 for K^0 and 0.95 for Λ. The distance of closest approach from the V^0 direction to the primary vertex is required to be less than 1.0 cm in the transverse plane. The specific ionization, dE/dx, on each track of a V^0 candidate is required to be within three standard deviations of the expected ionization. This requirement is only made if a useful measurement of the ionization of a track is available, i.e. when at least 50 ionization samples are measured by the TPC.

The mass spectra at this level of the event selection are shown in Figure 1. From these distributions a signal can be extracted in a momentum dependent mass window spanning more than 98% of the signal. The window size (in GeV/c^2) is $0.014 + 0.15 \cdot z$ for K^0 and $0.01 + 0.085 \cdot z$ for Λ, where z is the fraction of the beam momentum carried by the V^0.

A significant reduction of background is obtained by requiring a successful kinematical V^0 fit, constrained by the mass hypothesis and the primary vertex in the transverse plane [18]. This increases the number of degrees of freedom in the V^0 fit to three. The χ^2 of the fit is required to be less than 120. This requirement is very loose to minimize the dependence on the simulation. All of these candidates must have a mass pull, $\Delta M/\sigma_M$, less than four. If more than one V^0 hypothesis is available for the same charged tracks, a choice is made between them. For 4% of the K^0 candidates and 14% of the Λ candidates there is another candidate sharing one or both tracks, with the same mass hypothesis. Among these, the fit with the best χ^2 is chosen. For 2% of the K^0 candidates and 23% of the Λ candidates there is another candidate sharing both tracks, but with a different mass hypothesis. In this case, the fit with the smallest mass pull is chosen. The bias introduced by this method is corrected with the help of the Monte Carlo which reproduces well the number of such ambiguities.

4 Cross-section measurement

The cross-section measurement is presented as follows:

$$\begin{aligned} \frac{1}{\sigma_{had}}\frac{d\sigma}{d\xi} &= \frac{1}{\Delta\xi}\frac{n-b}{a} \\ \xi &= -\ln(p/p_{beam}) \end{aligned}$$

where n is the number of candidates selected by the kinematic fit per hadronic event in each bin of ξ, and p is the momentum. In addition, the cross–sections are presented as functions of transverse momentum and rapidity with respect to the thrust axis.

The acceptance, a, and the background, b, are calculated using a Monte Carlo simulation of hadronic events based on the event generators DYMU [19] and JETSET 7.3. The parameters of the hadron level simulation have been optimized to fit global event properties and lepton spectra measured in ALEPH [20, 21]. A detailed simulation of the apparatus was then carried out.

The size of the background is subsequently scaled by a factor $\alpha(\xi) = b_{DATA}/b_{MC}$, which is the ratio of background counts in the mass sidebands shown in Figure 1. This bin-by-bin correction factor has an average value of 1.0 for both particle types and never exceeds 20% .

The acceptance for charged decays and the background fraction are shown in Figure 2. The acceptance drops at high momentum due to the finite size of the TPC and the two–track resolution; it also drops at low momentum due to the threshold of about 150 MeV/c for reconstructing a track in the TPC. The background increases at high momentum due to the widening mass resolution, and at low momentum owing to the decreasing rejection power of the lifetime requirement and the vertex constraint. At the peak of the ξ spectrum, the acceptance (in the region of polar angles $20° < \Theta < 160°$) is 55% for K^0 and 53% for Λ, and the background fraction is 1.6% for K^0 and 7% for Λ.

5 Systematic errors

Systematic errors in this measurement arise from features which are not simulated correctly in the Monte Carlo. Such features can be divided into track reconstruction efficiencies, efficiencies of the V^0 finding and background calibration.

Track finding

A special problem may arise in the track reconstruction of V^0 tracks because of the two–track resolution. The measured angle between the daughter tracks has been compared with the simulation and found to be in good agreement in all projections. Also the number of measured TPC coordinates and the angular distribution of the V^0 candidates agree well with the simulation. Small deviations from the simulation are seen at low momentum. These give rise to a momentum dependent systematic error which is zero at high momentum and reaches 0.4% at the lowest momenta.

V^0 finding

As a check on the kinematic fit method, the V^0 candidates were alternatively selected using the mass windows shown in Figure 1. Using this method, the measured rate of K^0 increases by 0.6% and the rate of Λ increases by 2.5%. This raises the question of whether Λ from Ξ decays are rejected more strongly by the kinematic fit method which contains a vertex constraint. However, the number of Λ from Ξ in the final sample is 12% , according to the Monte Carlo simulation, compared with 14% before any

selection. Since the Ξ rate in JETSET agrees with the measured rate within a few percent [3, 24], this extra suppression of Λ from Ξ is not expected to contribute significantly to the errors.

Additional error contributions are obtained from varying the selection criteria. The requirement that the V^0 should point back to the primary vertex gives rise to the largest variation in the result, due to imperfect simulation of the impact parameter for low momentum V^0 candidates. All the variations obtained are added in quadrature, including the difference between the kinematic fit method and the mass window method. Part of the error depends on momentum, varying from 1% at 15 GeV/c to 4% at 0.7 GeV/c. In addition there is an overall normalisation error, which is 2% for K^0 and 3% for Λ.

Background

The selected sample of hadronic Z decays contains a small background of τ and two–photon final states [17]. These final states contain fewer V^0 than the hadronic events and lead to corrections of 0.4% and 0.6% for the K^0 rate and the Λ rate, respectively.

The error on the V^0 background is already included in the statistical errors, since the size of the background is taken from data. An additional error is obtained from varying the sidebands in the mass distributions, and this amounts to 0.2% for K^0 and 1.2% for Λ. No significant excess of Λ over $\bar{\Lambda}$ is seen at low momenta, hence errors from the simulation of nuclear interactions in the detector are neglected.

In total, the overall normalisation error is estimated to be 2% for K^0 and 4% for Λ. A correlated momentum–dependent relative systematic error, parametrized as $(0.04 \cdot \xi^2 + 0.8 \cdot \xi)\%$, is also to be added to the statistical errors shown in Table 1.

6 Differential cross–sections

The differential cross-sections are shown in Figure 3 and in Table 1. Predictions of JETSET and HERWIG are shown together with the measurements. The parameters of the models have been tuned to best reproduce ALEPH data [20, 21]. However, the strangeness suppression parameters are kept at their default values and the data on K^0 and Λ production have not been used in the tuning. The measured spectrum of K^0 is harder than the predicted spectra of both models, whereas the measured spectrum of Λ is softer than the model predictions. In particular, HERWIG has a leading particle effect for high momentum Λ which is not present in the data. The comparison with other experiments in Figure 4 shows a reasonable agreement between this and other measurements of the K^0 and Λ differential cross–sections.

The transverse momentum spectra and the rapidity spectra with respect to the thrust axis are shown in Figures 5 and 6 and in Table 2. The thrust axis is determined using the measured flow of both charged and neutral energy in the detector. Resolution effects are taken into account using the Monte Carlo simulation, so that the thrust axis corresponds to the one obtained from all particles at hadron level, except the neutrinos. Compared with JETSET, the K^0 data have a 14% larger average transverse momentum, while the Λ data are in reasonable agreement.

7 Average multiplicities

The contents of Table 1 are integrated from $\xi = 0$ to $\xi = 5.4$ (4.4 for Λ). The JETSET spectrum is used to extrapolate the average multiplicities from the momentum cutoff to zero, after normalising it to data in the interval $5 < \xi < 5.4$ ($4 < \xi < 4.4$ for Λ). The results are shown in Table 3, both for single particles and for pair combinations of K^0_S and Λ.

In addition to the systematic errors described above, an error is added for the extrapolation to zero momentum. The extrapolation contributes 0.013 to the K^0 multiplicity and 0.014 to the Λ multiplicity. The error is taken as the difference in this number between using HERWIG and JETSET for the extrapolation, which is 0.3% for K^0 and 0.5% for Λ. The spectrum at low momenta is dominated by contributions from resonances whose abundances differ significantly in JETSET and HERWIG.

For particle pairs an average acceptance is used, i.e. the number of pairs found in the simulation divided by the generated number of pairs. To account for the difference between the measured and generated spectra, which affects the extraction of the average acceptance, a correction of -2.0% was applied to each K^0 in a pair and a correction of -1.3% was applied to each Λ. The relative systematic errors on the multiplicities of each particle are added linearly and the full size of the above–mentioned correction is added in quadrature to obtain the systematic errors on the pair rates. Both for single particle multiplicities and for pair multiplicities the total errors are dominated by the systematic errors.

The results for the total K^0 and Λ multiplicities are compared with the previous measurements by OPAL [2, 3, 8], DELPHI [4, 5] and L3 [6] in Table 3. While the K^0 multiplicity and $\Lambda\bar{\Lambda}$ pair multiplicity is found to be in good agreement with the previous measurements, the Λ and $\Lambda\Lambda$ rates are somewhat larger than in references [3, 8, 5]. In Table 4 the measured multiplicities are compared with the predictions of JETSET and HERWIG. The agreement is good in general, except that HERWIG overestimates the Λ rate and in particular the $\Lambda\bar{\Lambda}$ pair rate. As also shown in Table 4, the total pair multiplicities already indicate a two–particle correlation (or anticorrelation in the case of $\Lambda\Lambda$ pairs).

8 Two–particle rapidity correlations

The two–particle correlation as a function of rapidity is here defined as:

$$C(y_a, y_b) = N_{had}\ \frac{n(y_a, y_b)}{n(y_a)n(y_b)}$$

where y is the rapidity along the thrust–axis. N_{had} is the number of hadronic events considered, $n(y_a, y_b)$ is the density of particle pairs with one particle at rapidity y_a and the other one at y_b, and $n(y)$ is the single particle density. The background, estimated from Monte Carlo simulation, is subtracted from each bin of the rapidity densities.

The correlation function is to first order independent of acceptance. The measured function is nevertheless corrected by a factor obtained from Monte Carlo simulation:

$$r(y_a, y_b) = \frac{C(y_a, y_b)_{hadron\ level}}{C(y_a, y_b)_{detector\ level}}$$

One reason for this correction, which is maximally $\pm 20\%$, is the smearing of the thrust axis direction by the experimental reconstruction (by 0.016 in $\cos\Theta_T$ and 0.04 in ϕ_T). Other second–order effects may also cause a difference between the acceptance of a pair of particles and the product of the single particle acceptances. The corrected results are shown in Figure 7 as a function of y_a for two choices of y_b: $0.5 < y_b < 1.5$ and $2.5 < y_b < 3.5$.

The main features of the rapidity correlations seen in Figure 7 are a strong short range correlation for $\Lambda\bar{\Lambda}$, a weaker one for $K^0_S K^0_S$ and ΛK^0_S and a short range *anti*-correlation for $\Lambda\Lambda$. These structures are all well reproduced by JETSET, whereas HERWIG overestimates the $\Lambda\bar{\Lambda}$ correlation by a factor of two.

Figure 8 shows the correlation function projected along rapidity difference. This distribution is obtained by dividing the distribution of rapidity differences by that of two particles taken from different

events. The denominator is normalized to the number of pairs expected in case of no correlations. Corrections for background and resolution are applied as explained above.

Also shown in Figure 8 are the correlation functions predicted by JETSET for various popcorn parameters and by HERWIG. The $\Lambda\bar{\Lambda}$ data is found consistent with JETSET with the standard popcorn probability of 50% and less consistent with the option having no popcorn mechanism. The systematic errors of the measurement prevent more quantitative statements. Similar studies by OPAL [8] and DELPHI [5] have also concluded that a significant amount of popcorn contribution in JETSET is needed to reproduce the measured rapidity differences.

Since the average $\Lambda\bar{\Lambda}$ and $\Lambda\Lambda$ pair multiplicity is also quite sensitive to the popcorn parameter, it can be used as a consistency check. The predicted multiplicity of Λ pairs decreases approximately linearly with the popcorn probability. The measured multiplicity thus constrains the popcorn probability to be within the range: 0.50 ± 0.10 (assuming this to be the only free parameter affecting the Λ pair multiplicity). In conclusion, the data gives no reason to change the default 50% popcorn probability in JETSET.

9 Angular correlations relative to thrust–axis

In the following, the particle pairs are restricted to the interval $\Delta y < 1.5$ and the structure of the short range correlation is studied as a function of other variables. The same procedure as used for rapidity differences is now used to find the correlation as a function of $\Delta\phi$, where ϕ is the azimuthal angle around the thrust axis. This is shown in Figure 9.

For $\Lambda\bar{\Lambda}$ pairs, a large peak is seen at $\Delta\phi = 0°$, and no significant peak is seen at $\Delta\phi = 180°$. Hence there is no hint of local p_T compensation among correlated $\Lambda\bar{\Lambda}$ pairs. This is in contrast to observations at center–of–mass energies around 10 GeV, where baryon–antibaryon pairs are predominantly back–to–back in azimuth [22]. At PETRA energies there is an intermediate situation with no prominent peaks neither at $\Delta\phi = 0°$ nor at $\Delta\phi = 180°$ [11]. For the other two–particle combinations, both a same–side and a back–to–back correlation is seen. All of these features are well reproduced by JETSET, and not so well by HERWIG which predicts a strong back–to–back correlation in the case of $\Lambda\bar{\Lambda}$ pairs. The predicted correlations do not depend significantly on the popcorn probability.

Another interesting variable is the polar angle of the $\Lambda\bar{\Lambda}$ pair in its rest frame relative to the thrust axis. The normalised angular distribution shown in Figure 10 shows an alignment of the $\Lambda\bar{\Lambda}$ pair along the thrust axis. This effect has previously been reported by DELPHI [5] and was also found earlier at lower energies in $p\bar{p}$ pairs [9]. In JETSET the baryon pairs are aligned along the parent string, and this model reproduces data. The HERWIG clusters, on the other hand, decay isotropically. A version of HERWIG introducing an anisotropy by letting clusters containing a quark from the perturbative shower decay in the direction of this quark [23] is also shown in Figure 10, but this is apparently not enough to describe the data.

10 Bose-Einstein correlation

Part of the observed short range correlation in the $K^0_S K^0_S$ system could be due to Bose-Einstein correlation (BEC), which has been observed in this system by OPAL [7] and DELPHI [28] using the JETSET model as a reference sample without BEC. In Figure 11 the $K^0_S K^0_S$ correlation is shown as a function of $Q = \sqrt{M^2_{KK} - 4m^2_K}$, also using JETSET as the reference sample. The corrected Q distribution of the data is divided by the distribution of the generator. The ratio is normalised in the interval between

0.6 GeV and 2.5 GeV (excluding the range 1.1 GeV to 1.5 GeV where resonances such as $f_2'(1525)$ and $f_0(1710)$ may contribute). The ratio is fitted to a four–parameter expression of the form:

$$C(Q) = N(1+\delta\cdot Q)(1+\lambda\cdot\exp(-Q^2(R_0/0.197)^2)$$

where R_0 is the radius of the K^0 emitting region (in fermi), and λ is the chaosity parameter or correlation strength. The δ parameter is introduced to allow for the measured deviations from the generated K^0 spectrum.

The result is shown in Table 5. The fit is good and yields a source size of 0.71 ± 0.07 fm, where the error is statistical, and a correlation strength of 1.4 ± 0.3. If the generator distribution is reweighted so as to reproduce the measured p_T spectrum of the K^0 mesons, then the δ parameter is reduced by roughly a factor of two, while the radius and strength parameters stay the same. Replacing the JETSET reference sample with HERWIG also leaves the radius and strength parameters the same.

The scalar mesons $f^0(975)$ and $a_0(980)$ are not produced in the default version of JETSET. Correcting for the f^0 as described in reference [28], the fitted source size is reduced to 0.65 fm and the strength parameter to 1.0. The uncertainties in the f^0 width and rate give rise to a systematic error of 0.05 fm on the size and 0.3 on the strength. The rate and branching ratios of the a_0 meson are unknown.

Systematic errors from sources other than the scalar resonances are found by varying the parameters in the JETSET model, the fit range, the parametrisation of the correlation and the event selection. Thus, the systematic error on the radius is estimated to 0.15 fm, and the systematic error on the correlation strength is similarly estimated to be 0.40. Table 5 indicates good agreement with the OPAL and DELPHI measurements of the radius and correlation strength.

11 Discussion and summary

From Figures 3, 5 and 6 it is seen that the measured K^0 spectrum is significantly harder than the predicted spectrum from both JETSET and HERWIG. The peak of the ξ–distribution is located at a value 0.22 lower than JETSET, and the average transverse momentum is 14% higher than the JETSET prediction. No consistent choice of parameters in JETSET has been found which reproduces the K^0 spectrum perfectly. However, reasonable agreement at low momenta is obtained by enabling the production of tensor mesons in JETSET and by suppressing the rate of strange vector mesons so that it agrees with measurements of K^* production [27, 25, 4]. At higher momenta, $1 < \xi < 2.2$, the contribution from heavy flavor decays is important, and the prediction depends on the proper implementation of decay branching fractions in the generators.

The Λ spectrum is in reasonable agreement with the JETSET prediction – except at the highest momenta where the predicted yield is too large, as also found by previous measurements [3, 5]. The HERWIG yield is generally too large. In particular, HERWIG has a shoulder at high momenta, which is not visible in the data. This is caused by a large yield of Λ containing a primary quark in HERWIG. The model has also a large yield of Λ at low momenta. This is caused by the very large rate of Ξ states and of spin 3/2 baryons in HERWIG. Such heavy baryons are produced more than twice as frequently in the default version of HERWIG than in JETSET. The measured Λ spectrum does not support a copious production of heavy hyperons, and neither do direct measurements of Ξ and Σ production [3, 24].

The correlations as a function of rapidity and azimuth relative to the thrust axis within pairs of Λ and K^0 are found to be in good agreement with JETSET. Also HERWIG reproduces many of the features. However, the $\Lambda\bar{\Lambda}$ correlation disagrees with HERWIG, both in size – it is a factor of two smaller than predicted – and in qualitative features. One such feature is the degree of local p_T compensation shown in

Figure 9, where HERWIG predicts a sizeable back–to–back peak, while the data has none. Another feature is the angular distribution of the baryon–pairs in their rest frame, which is too isotropic in HERWIG.

The observed correlation length in $\Lambda\bar{\Lambda}$ indicates that some amount of the "popcorn" mechanism in JETSET is necessary to describe the data. The observed $\Lambda\bar{\Lambda}$ and $\Lambda\Lambda$ multiplicity is consistent with a popcorn probability of 0.50 ± 0.10, when all other parameters are held fixed.

Finally, a possible signal for Bose–Einstein correlation is observed using JETSET as a reference sample. The radius of the K^0 emitting region is estimated to 0.7 ± 0.2 fm, and the correlation has close to maximal strength. The signal suffers, however, from uncertainties in the rates and branching fractions of the scalar mesons $f^0(975)$ and $a_0(980)$.

Acknowledgement

We wish to thank our colleagues in the CERN accelerator division for operating the LEP machine. We are also grateful to the engineers and technicians in all our institutions for their contribution to the success of ALEPH. Those of us from non–member states thank CERN for its hospitality.

References

[1] For a review of jet fragmentation phenomenology at PEP and PETRA, see for example: W. Hofmann, Ann.Rev.Nucl.Part.Sci. **38**(1988)279 or T.Sjöstrand, Int.Jour.Mod.Phys **A3**(1988)751.

[2] (OPAL coll.), G.Alexander *et al.*, Phys.Lett **B264**(1991)467.

[3] (OPAL coll.), P.D.Acton *et al.*, Phys.Lett **B291**(1993)503.

[4] (DELPHI coll.), P.Abreu *et al.*, Phys.Lett **B275**(1992)231.

[5] (DELPHI coll.), P.Abreu *et al.*, Phys.Lett. **B316**(1993)253.

[6] (L3 coll.), M.Acciarri *et al.*, preprint CERN-PPE/94-53.

[7] (OPAL coll.), P.D.Acton *et al.*, Phys.Lett **B298**(1993)456.

[8] (OPAL coll.), P.D.Acton *et al.*, Phys.Lett **B305**(1993)415.

[9] (TPC coll.), H.Aihara *et al.*, Phys.Rev.Lett. **55**(1985)1047.

[10] (TASSO coll.) M. Althoff et al., Phys.Lett. **B139**(1984)126.

[11] (TASSO coll.) M. Althoff et al., Z.Phys **C17**(1984)5.

[12] T.Sjöstrand and M.Bengtsson, Comp.Phys.Comm. **39**(1986)367.

[13] G.Marchesini, B.R.Webber, G.Abbiendi, I.G.Knowles, M.H.Seymour and L.Stanco, Comp. Phys. Comm. **67**(1992)465.

[14] (ALEPH coll.), D.Decamp *et al.*, Nucl.Instr.Meth. **A294**(1990)121.

[15] W.Atwood *et al.*, Nucl.Instr.Meth. **A306**(1991)446.

[16] G.Batignani *et al.*, Proc. 1991 IEEE Nucl. Sci. Symposium, Santa Fe.

[17] (ALEPH coll.), D.Decamp *et al.*, Z.Phys **C53**(1992)1.

[18] B.Rensch, "Produktion der neutralen seltsamen Teilchen K^0 and Λ in hadronischen Z–Zerfällen am LEP–Speicherring", PhD Thesis, Universität Heidelberg, Sept 1992.

[19] J.E.Campagne, Ph.D. Thesis (Paris), preprint LPNHEP 89-02. J.E.Campagne and R.Zitoun, Z.Phys. C43(1989)469.

[20] (ALEPH coll.), D.Busculic *et al.*, Z.Phys **C55**(1992)209.

[21] (ALEPH coll.), D.Busculic *et al.*, preprint CERN-PPE/94-017.

[22] (ARGUS coll.), H.Albrecht *et al.*, Z.Phys **C43**(1989)45.

[23] B.R.Webber, private communication.

[24] (ALEPH coll.), D.Busculic *et al.*, 'Hyperon production in Z decays', contributed paper to ICHEP 1992, Dallas.

[25] (DELPHI coll.), P.Abreu *et al.*, Phys.Lett. **B298**(1993)236.

[26] (OPAL coll.), P.D.Acton *et al.*, Z.Phys. **C56**(1992)521.

[27] (OPAL coll.), P.D.Acton *et al.*, Phys.Lett. **305B**(1993)407.

[28] (DELPHI coll.), P.Abreu *et al.*, preprint CERN-PPE/94-03.

ξ	$\frac{1}{\sigma_{had}}\frac{d\sigma}{d\xi}$ K^0	$\frac{1}{\sigma_{had}}\frac{d\sigma}{d\xi}$ Λ
0.0 – 0.2	0.008 ± 0.006	0.0008 ± 0.0008
0.2 – 0.4	0.028 ± 0.005	0.0031 ± 0.0009
0.4 – 0.6	0.067 ± 0.006	0.0116 ± 0.0015
0.6 – 0.8	0.118 ± 0.006	0.028 ± 0.002
0.8 – 1.0	0.185 ± 0.006	0.041 ± 0.002
1.0 – 1.2	0.274 ± 0.007	0.057 ± 0.002
1.2 – 1.4	0.361 ± 0.007	0.074 ± 0.002
1.4 – 1.6	0.450 ± 0.007	0.092 ± 0.002
1.6 – 1.8	0.543 ± 0.007	0.102 ± 0.002
1.8 – 2.0	0.596 ± 0.007	0.116 ± 0.002
2.0 – 2.2	0.642 ± 0.007	0.126 ± 0.002
2.2 – 2.4	0.659 ± 0.007	0.133 ± 0.002
2.4 – 2.6	0.689 ± 0.007	0.139 ± 0.002
2.6 – 2.8	0.705 ± 0.007	0.143 ± 0.002
2.8 – 3.0	0.683 ± 0.007	0.146 ± 0.003
3.0 – 3.2	0.659 ± 0.007	0.143 ± 0.003
3.2 – 3.4	0.632 ± 0.007	0.127 ± 0.003
3.4 – 3.6	0.582 ± 0.007	0.114 ± 0.003
3.6 – 3.8	0.521 ± 0.007	0.088 ± 0.003
3.8 – 4.0	0.473 ± 0.007	0.077 ± 0.003
4.0 – 4.2	0.404 ± 0.007	0.061 ± 0.004
4.2 – 4.4	0.317 ± 0.007	0.043 ± 0.004
4.4 – 4.6	0.233 ± 0.007	
4.6 – 4.8	0.160 ± 0.007	
4.8 – 5.0	0.125 ± 0.007	
5.0 – 5.2	0.071 ± 0.007	
5.2 – 5.4	0.053 ± 0.007	
5.4 – 5.6	0.030 ± 0.013	

Table 1: The inclusive spectrum of $K^0_S + K^0_L$ and $\Lambda + \bar{\Lambda}$ from hadronic Z decay as a function of ξ. The errors are statistical. A correlated momentum dependent relative error of the form $(0.04\xi^2 + 0.8\xi)\%$ and an overall normalisation error of 2% for K^0 and 4% for Λ should be added.

p_T (GeV/c)	$\frac{1}{\sigma_{had}}\frac{d\sigma}{dp_T}$ K^0	$\frac{1}{\sigma_{had}}\frac{d\sigma}{dp_T}$ Λ
0.0 – 0.4	1.536 ± 0.017	0.176 ± 0.006
0.4 – 0.8	1.669 ± 0.016	0.303 ± 0.006
0.8 – 1.2	0.816 ± 0.009	0.184 ± 0.003
1.2 – 1.6	0.415 ± 0.006	0.104 ± 0.002
1.6 – 2.0	0.219 ± 0.004	0.0626 ± 0.0015
2.0 – 2.4	0.146 ± 0.004	0.0398 ± 0.0012
2.4 – 2.8	0.0911 ± 0.0023	0.0260 ± 0.0009
2.8 – 3.2	0.0617 ± 0.0018	0.0155 ± 0.0007
3.2 – 3.6	0.0426 ± 0.0016	0.0121 ± 0.0007
3.6 – 4.0	0.0301 ± 0.0014	0.0083 ± 0.0006
4.0 – 4.4	0.0219 ± 0.0012	0.0058 ± 0.0005
4.4 – 4.8	0.0152 ± 0.0011	0.0042 ± 0.0004
4.8 – 5.2	0.0113 ± 0.0007	0.0022 ± 0.0004
5.2 – 5.6	0.0116 ± 0.0030	0.0024 ± 0.0003
5.6 – 6.0	0.0070 ± 0.0006	0.00167 ± 0.00023
6.0 – 6.4	0.0068 ± 0.0007	0.00155 ± 0.00025
6.4 – 6.8	0.0037 ± 0.0005	0.00121 ± 0.00022
6.8 – 7.2	0.0027 ± 0.0004	0.00091 ± 0.00025
7.2 – 7.6	0.0027 ± 0.0005	0.00051 ± 0.00015
7.6 – 8.0	0.0022 ± 0.0005	0.00032 ± 0.00014
8.0 – 8.4	0.0027 ± 0.0013	0.00048 ± 0.00025
8.4 – 8.8	0.0019 ± 0.0010	0.00056 ± 0.00019
8.8 – 9.2	0.00087 ± 0.0031	0.00023 ± 0.00010
9.2 – 9.6	0.00068 ± 0.00020	0.00042 ± 0.00030
9.6 – 10.0	0.00059 ± 0.00020	0.00004 ± 0.00003
10.0 – 10.4	0.00032 ± 0.00013	0.00010 ± 0.00007
10.4 – 10.8	0.00022 ± 0.00012	0.00004 ± 0.00004
10.8 – 11.2	0.00028 ± 0.00017	0.00009 ± 0.00009
11.2 – 11.6	0.00096 ± 0.00082	0.00006 ± 0.00006
11.6 – 12.0	0.00059 ± 0.00050	0.00006 ± 0.00006

Table 2: The inclusive spectrum as a function of p_T of $K^0_S + K^0_L$ and $\Lambda + \bar{\Lambda}$ from hadronic Z decay. There is an additional normalisation error of 2% for K^0 and 4% for Λ.

$< n >$	ALEPH Data	DELPHI data	OPAL data	L3 data
$K^0_S + K^0_L$	2.061 ± 0.047	2.12 ± 0.07 [4]	2.10 ± 0.14 [2]	2.04 ± 0.14 [6]
$\Lambda + \bar{\Lambda}$	0.386 ± 0.016	0.357 ± 0.017 [5]	0.351 ± 0.019 [3]	0.37 ± 0.04 [6]
$\Lambda\bar{\Lambda}$	0.093 ± 0.009	0.090 ± 0.009 [5]	0.083 ± 0.010 [8]	
$\Lambda\Lambda + \bar{\Lambda}\bar{\Lambda}$	0.028 ± 0.003	0.018 ± 0.006 [5]	0.021 ± 0.005 [8]	
$\Lambda K^0_S + \bar{\Lambda} K^0_S$	0.403 ± 0.029			
$K^0_S K^0_S$	0.593 ± 0.036			

Table 3: Average multiplicities of Λ, K^0 and their two–particle combinations. The errors on the measurements are dominantly systematic.

$< n >$	ALEPH Data	Uncorr.	JETSET	Uncorr.	HERWIG	Uncorr.
$K^0_S + K^0_L$	2.061 ± 0.047		2.11		2.24	
$\Lambda + \bar{\Lambda}$	0.386 ± 0.016		0.394		0.449	
$\Lambda\bar{\Lambda}$	0.093 ± 0.009	0.037	0.092	0.039	0.192	0.050
$\Lambda\Lambda + \bar{\Lambda}\bar{\Lambda}$	0.028 ± 0.003	0.037	0.031	0.039	0.048	0.050
$\Lambda K^0_S + \bar{\Lambda} K^0_S$	0.403 ± 0.029	0.397	0.427	0.377	0.474	0.491
$K^0_S K^0_S$	0.593 ± 0.036	0.531	0.619	0.557	0.695	0.601

Table 4: Average multiplicities of Λ, K^0 and their two–particle combinations compared with model predictions. The columns labeled *Uncorr* contain the expectation if the particles belonging to the column on the left were produced uncorrelated.

Fit	χ^2	NDF	N	δ	R_0 (fm)	λ
ALEPH 4–param	6	21	0.76 ± 0.04	0.22 ± 0.04	0.71 ± 0.07	1.39 ± 0.26
Corrected for f^0	10	21	0.73 ± 0.04	0.25 ± 0.05	0.65 ± 0.07	0.96 ± 0.21
OPAL 2–param [7]	3.4	8			0.72 ± 0.17	1.12 ± 0.33
OPAL 4–param [7]	1.9	6	0.89 ± 0.11	0.10 ± 0.11	0.61 ± 0.16	1.17 ± 0.23
DELPHI [28]					0.90 ± 0.19	1.13 ± 0.54

Table 5: Results of $C(Q)$ fits to data in the range $0 < Q < 1.1$ and $1.5 < Q < 2.5$ GeV. The errors are statistical.

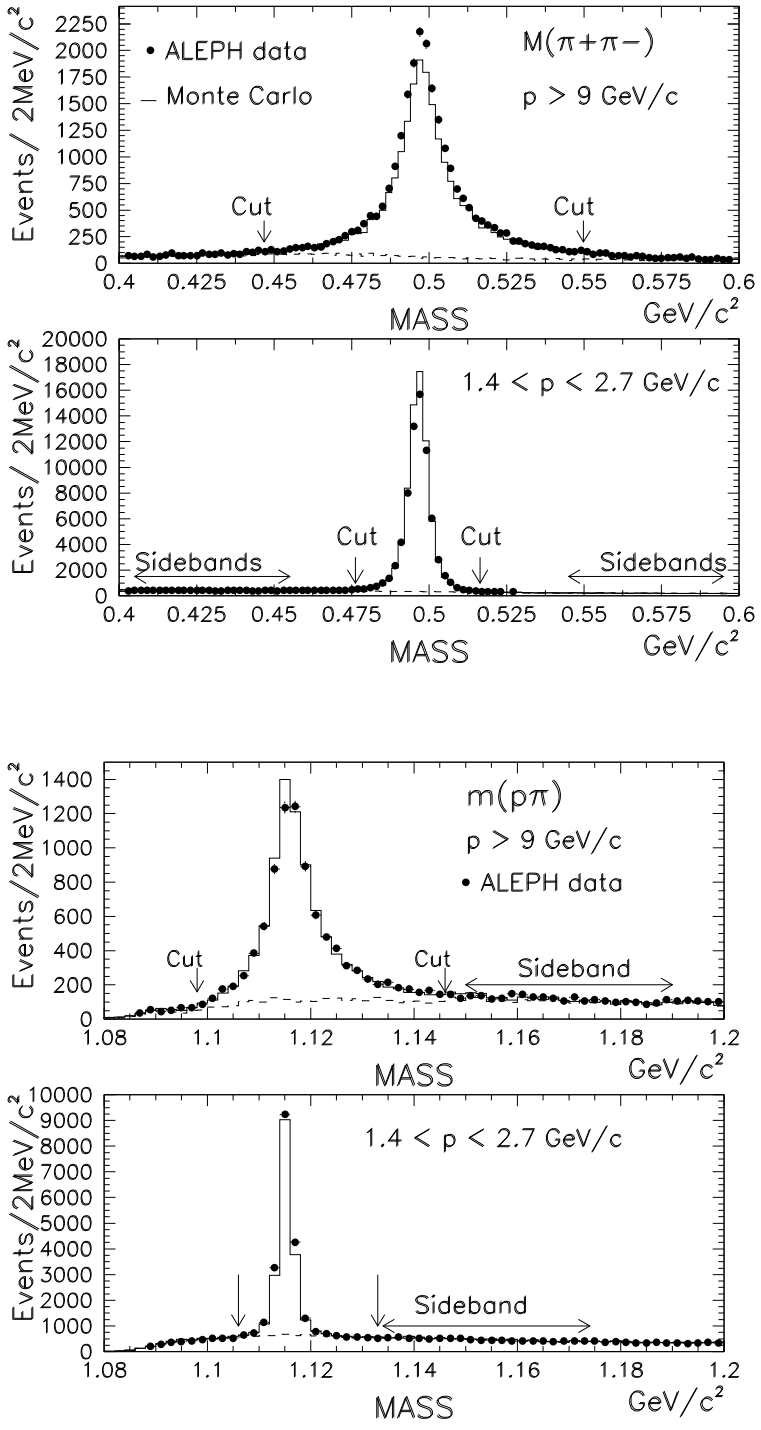

Figure 1: Invariant mass spectra of $\pi^+\pi^-$ and $p\pi$ combinations in two momentum intervals. The dots are the number of measured events, the solid line the simulated events and the dashed line is the expected background contribution.

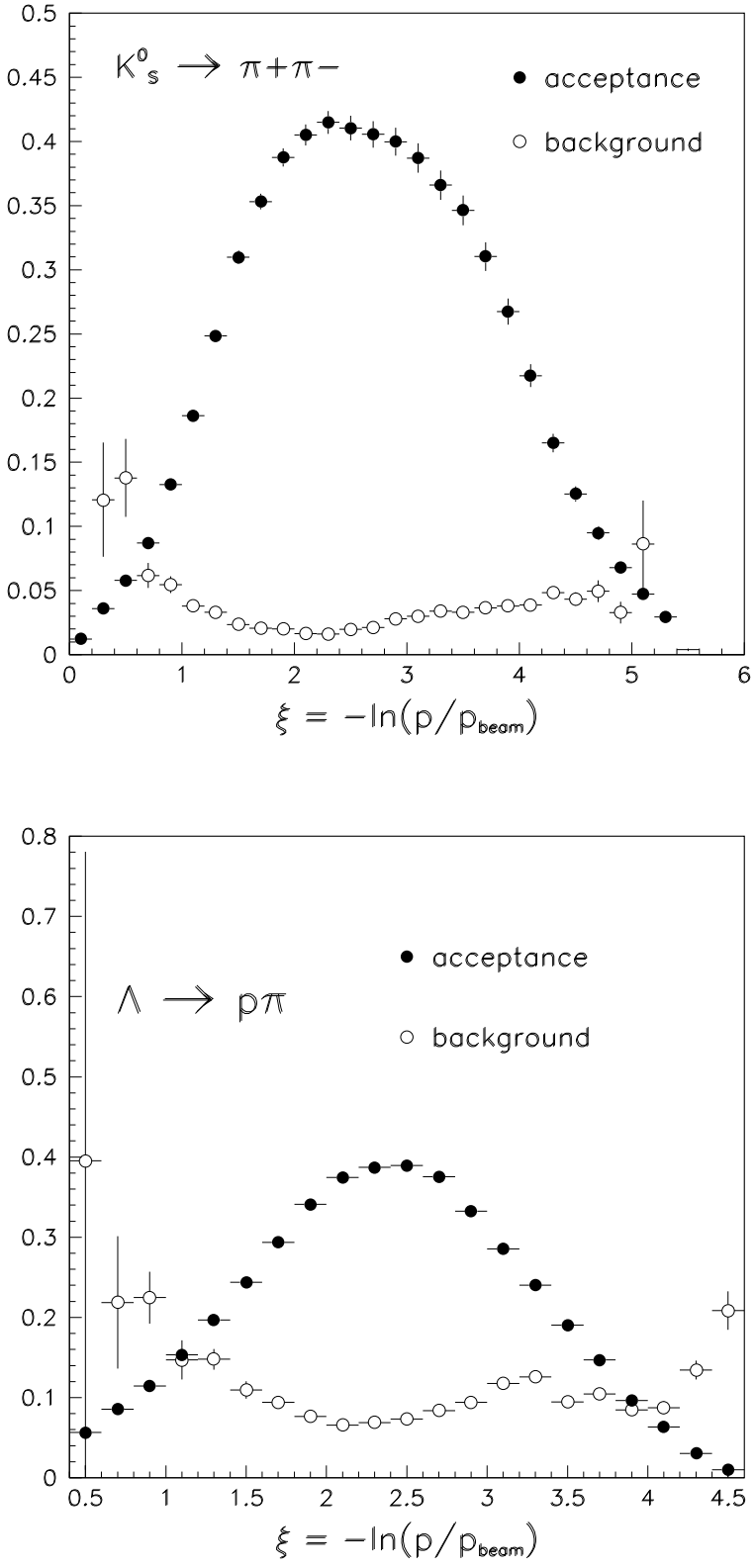

Figure 2: Acceptance for selecting charged V^0 decays and the background fraction of the selected sample.

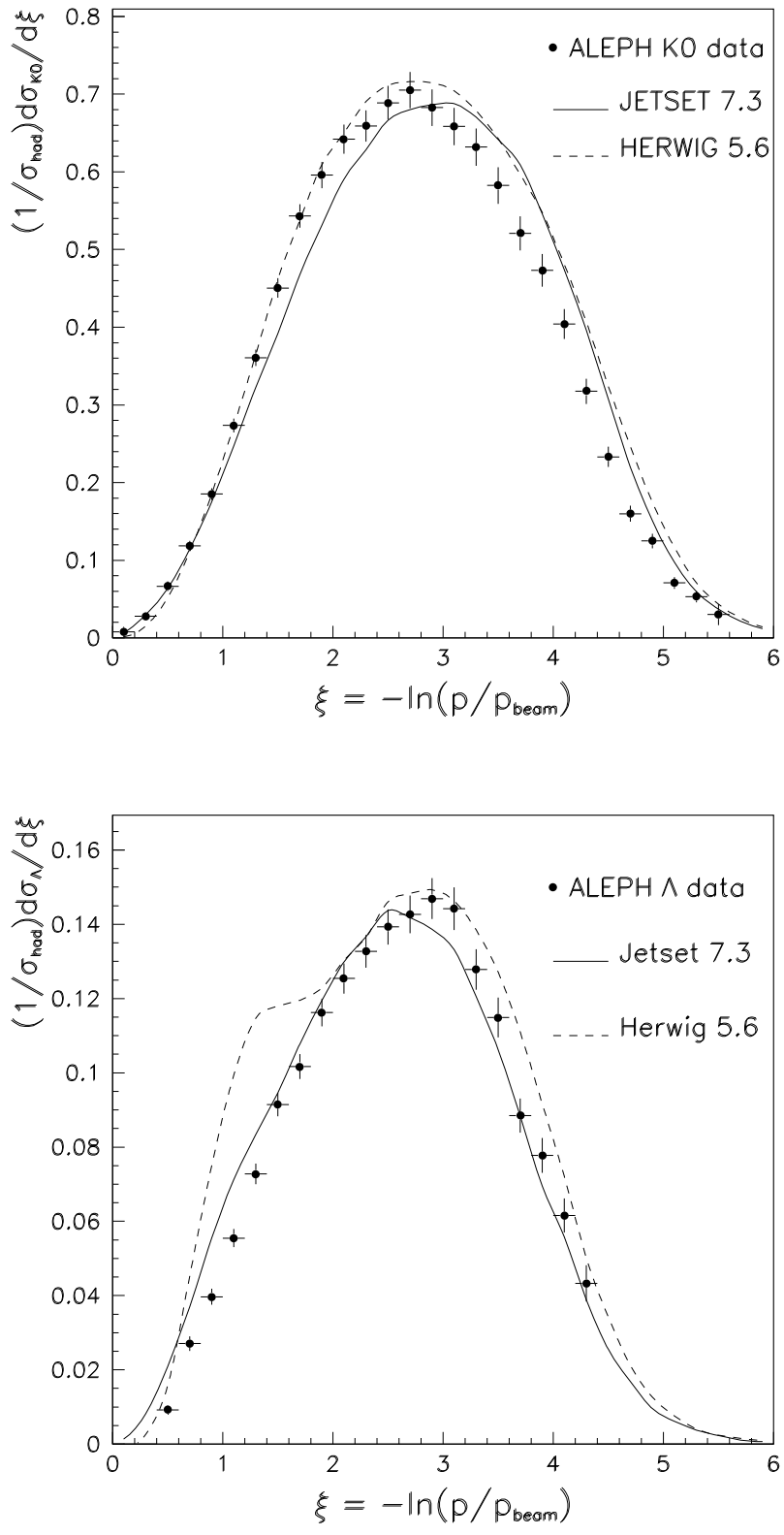

Figure 3: Momentum spectra of K^0 (upper) and Λ (lower). The systematic errors are added in quadrature. Note that the systematic errors are correlated errors.

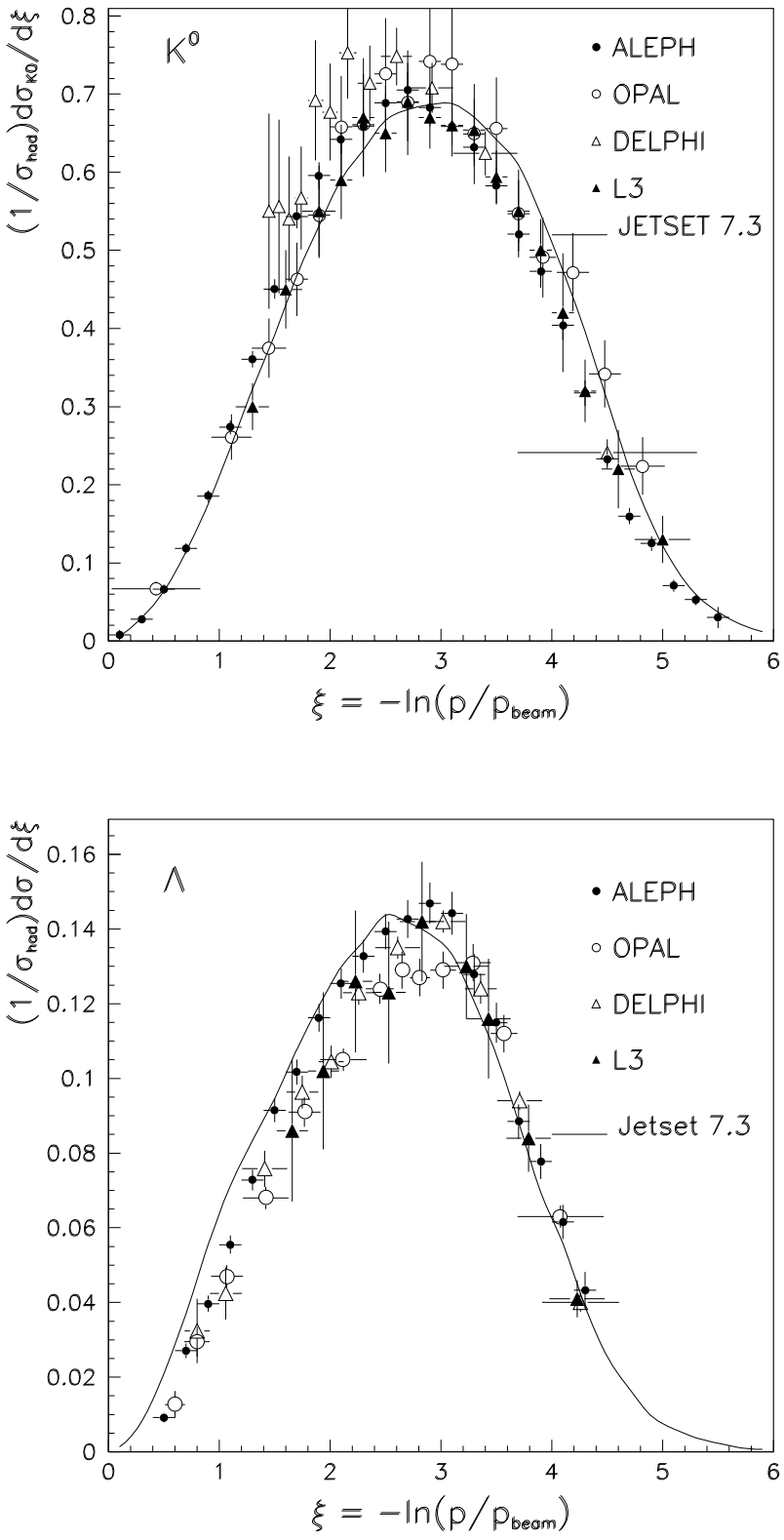

Figure 4: Momentum spectra of K^0 (upper) and Λ (lower) as measured by the four LEP experiments [2, 3, 4, 5, 6]. Systematic errors are added in quadrature.

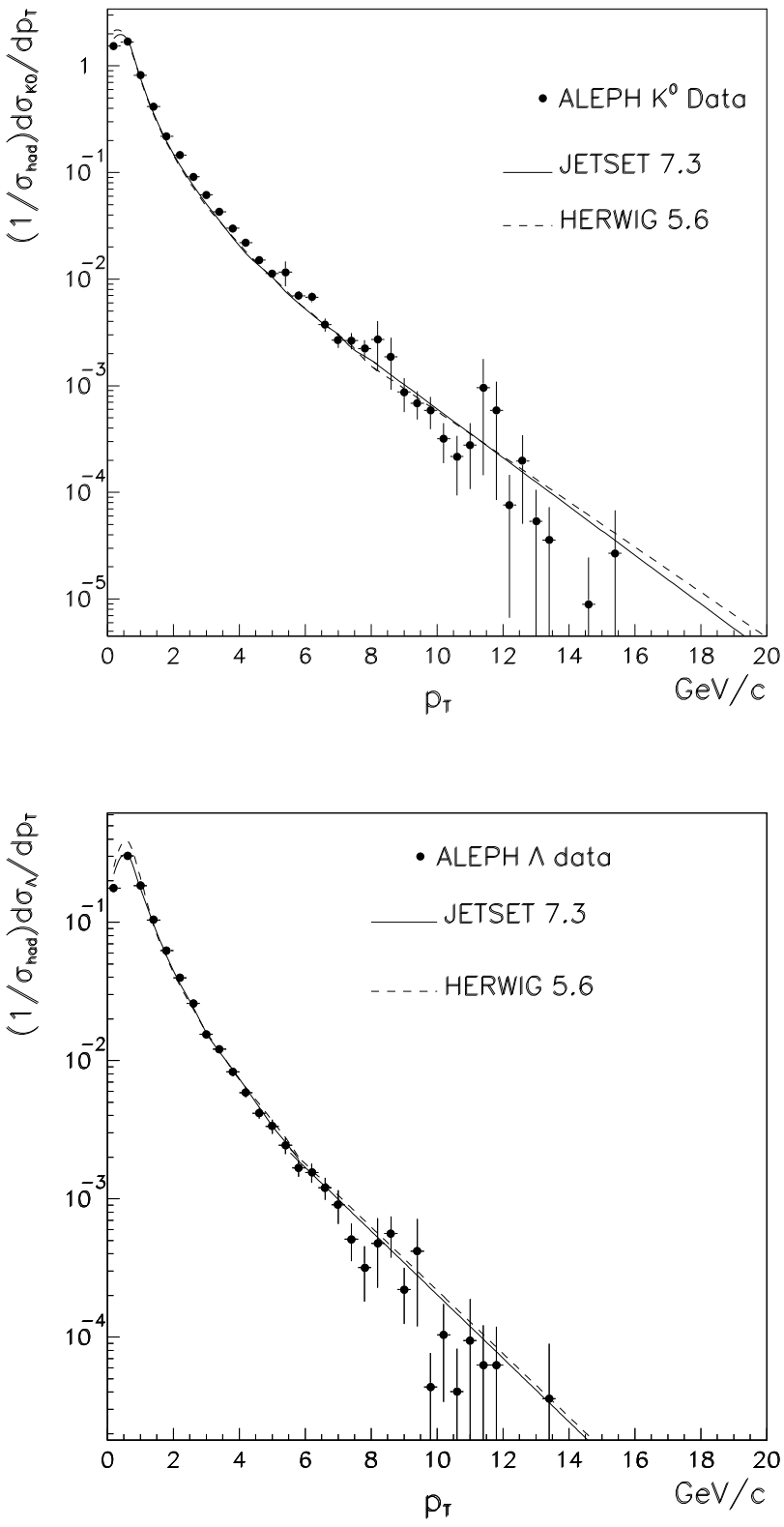

Figure 5: Transverse momentum spectra of K^0 (upper) and Λ (lower). Systematic errors are added in quadrature.

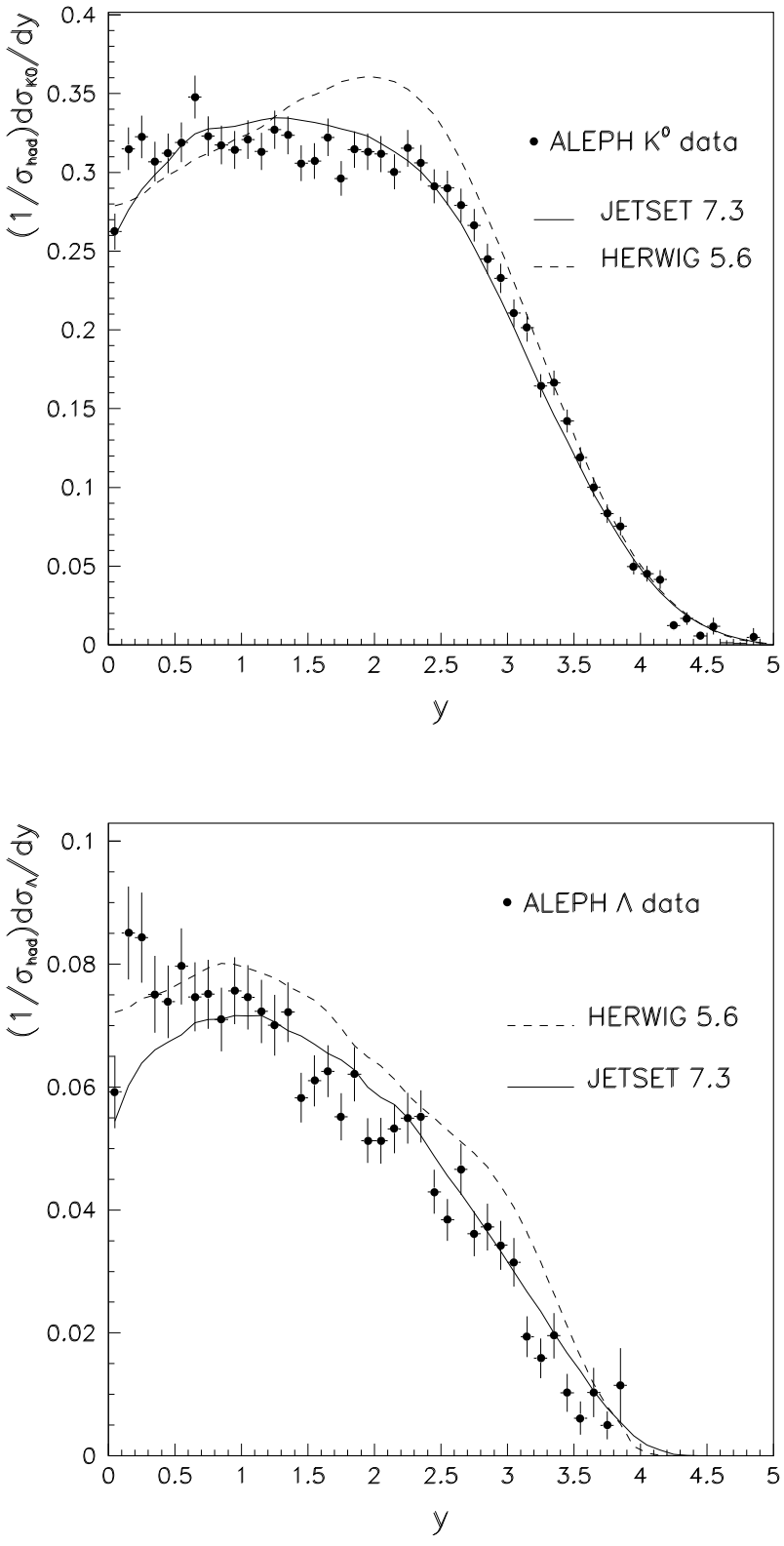

Figure 6: Rapidity spectra of K^0 (upper) and Λ (lower). Systematic errors are added in quadrature.

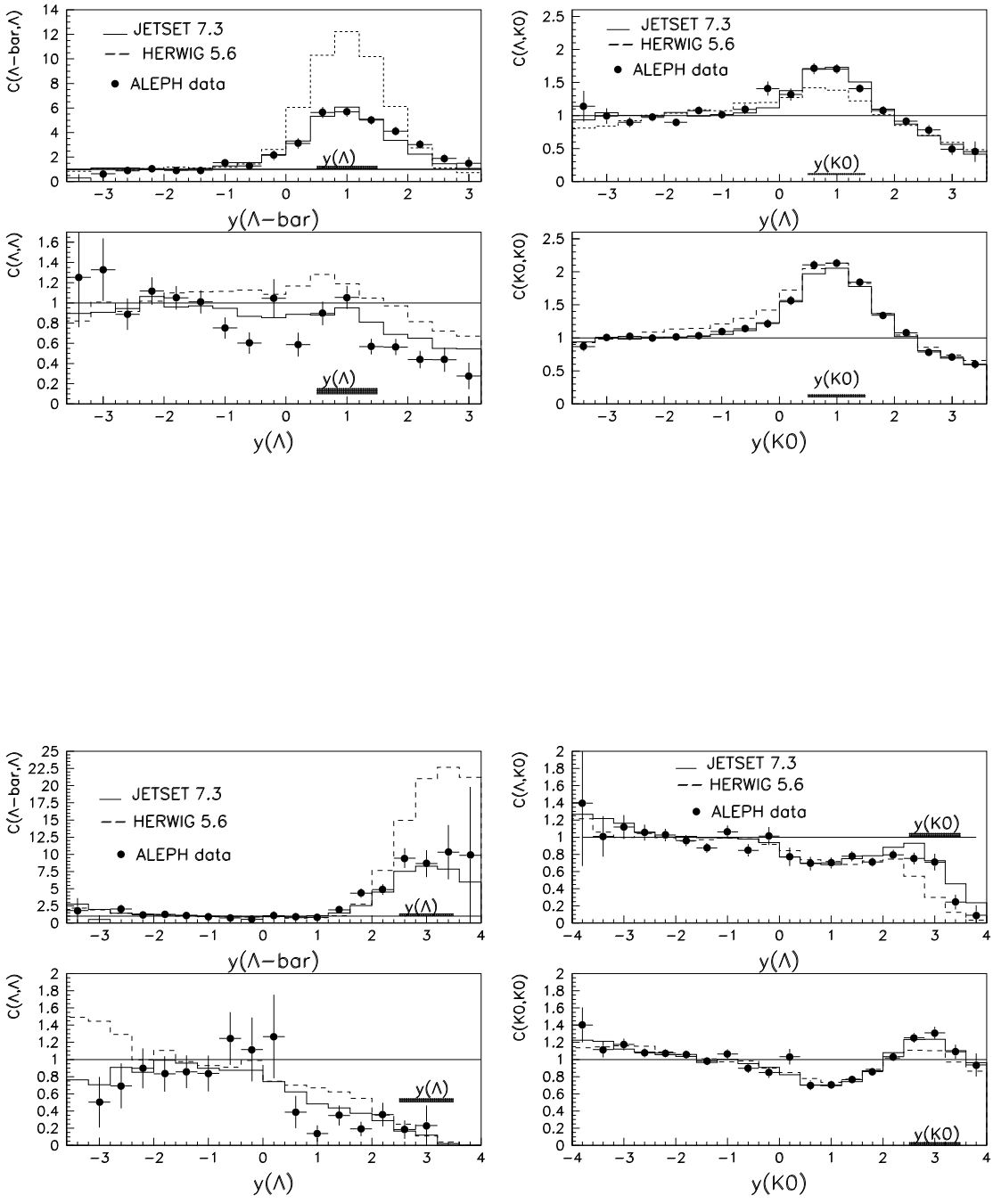

Figure 7: Two-particle correlation as a function of y_a for two y_b intervals.

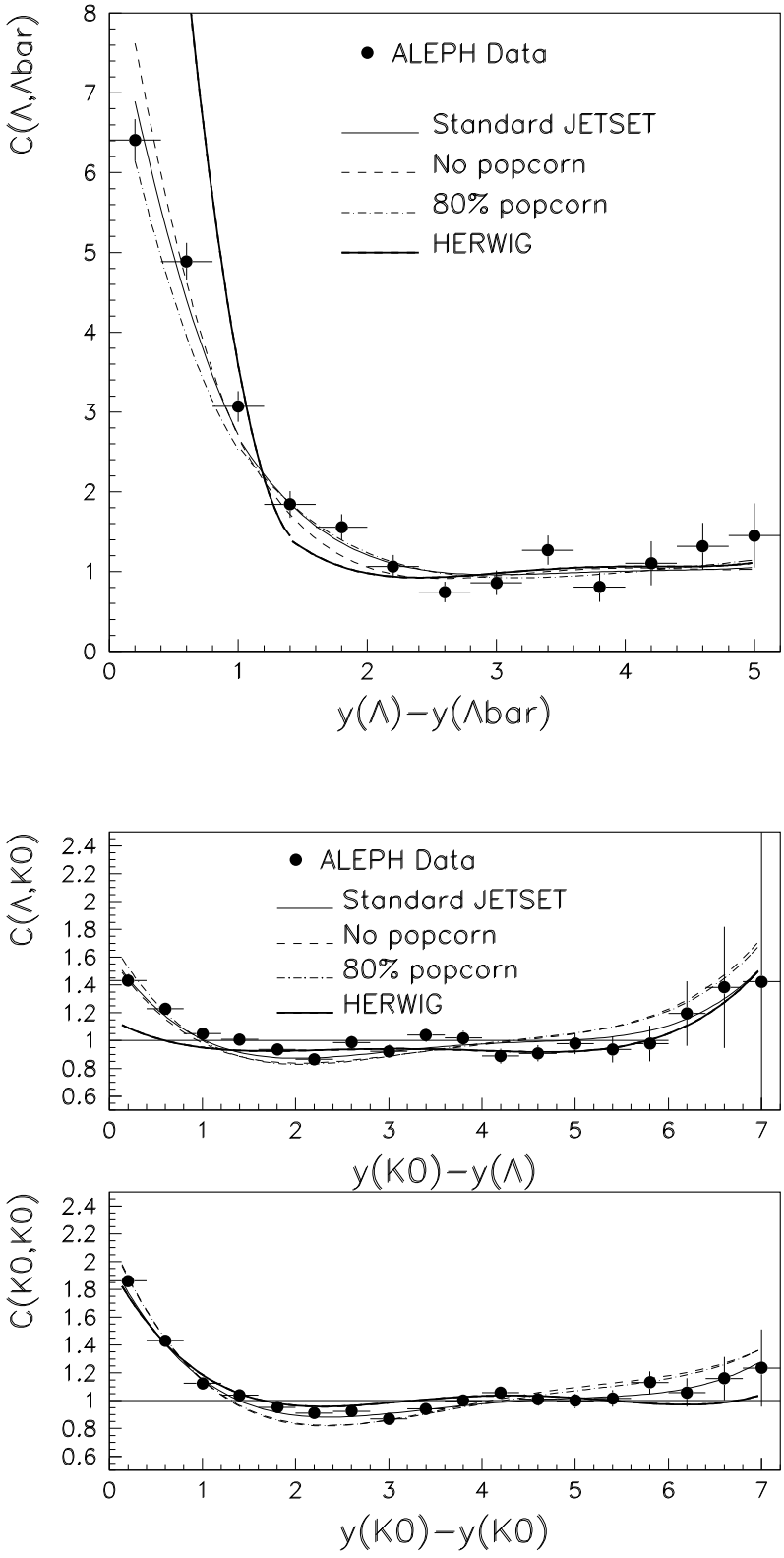

Figure 8: Two–particle correlations as a function of rapidity difference.

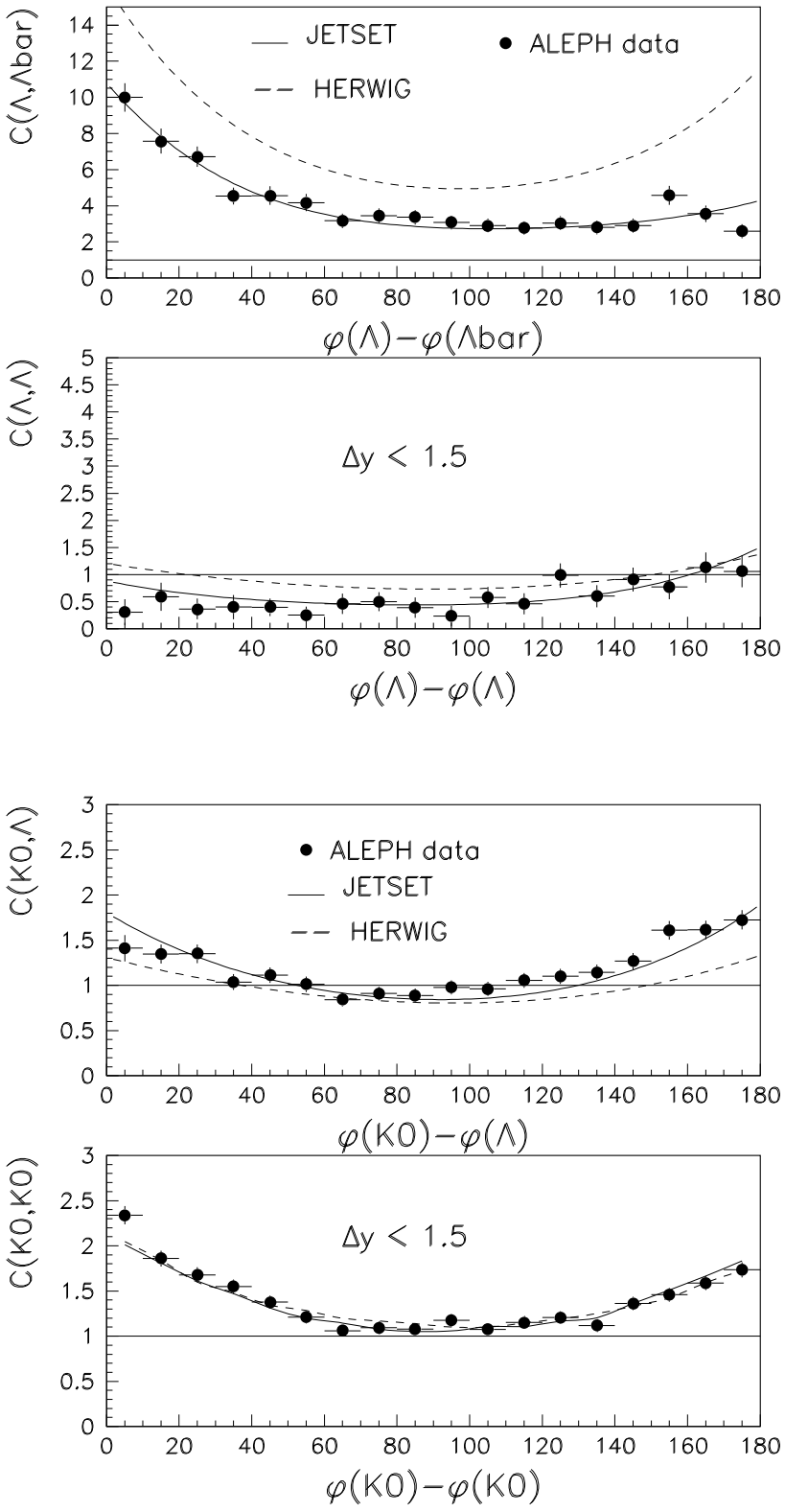

Figure 9: Two–particle correlations as a function of azimuthal separation.

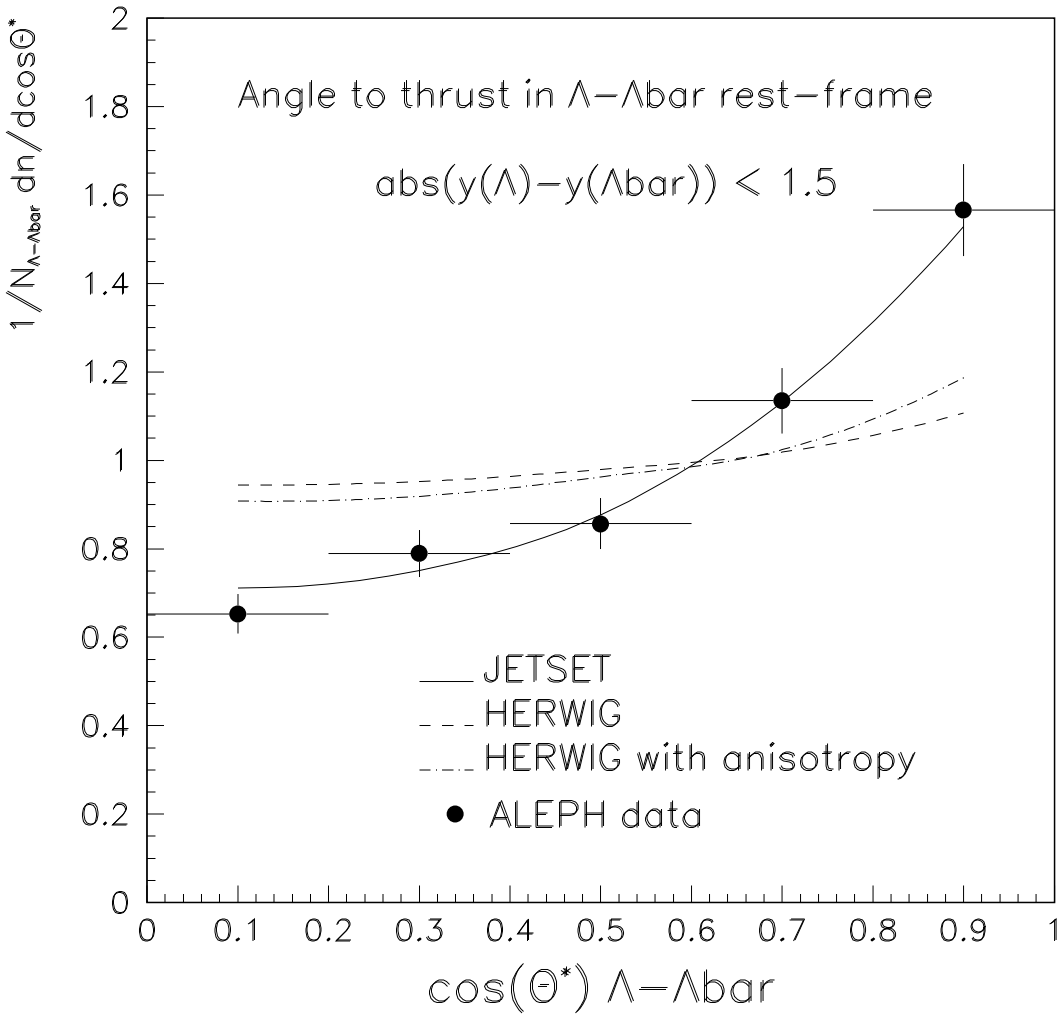

Figure 10: Angle of Λ to thrust axis in the $\Lambda\bar{\Lambda}$ restframe.

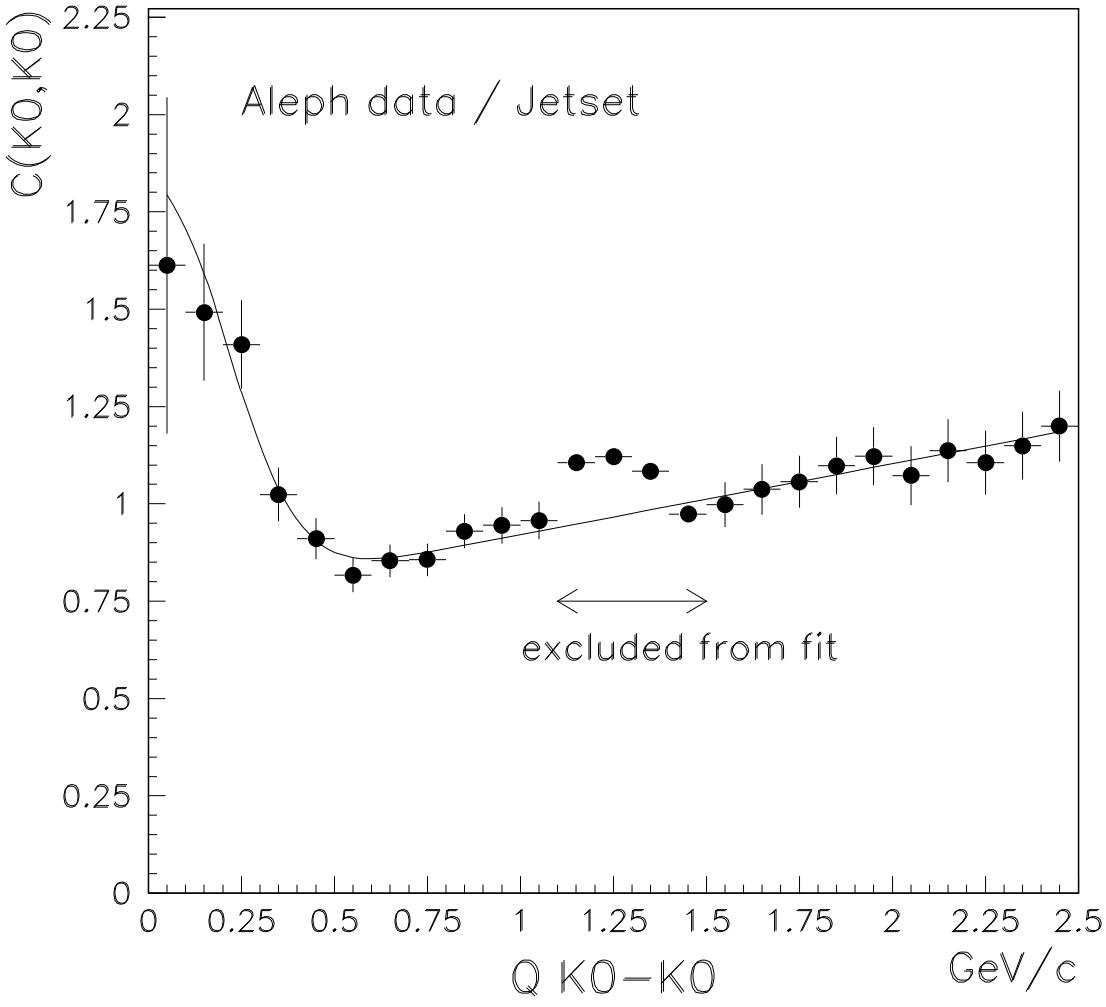

Figure 11: The $Q(K^0_S K^0_S)$ distribution divided by a generator distribution without Bose–Einstein correlation.